Supporting information

Selective growth of graphene-confined inkjet-printed Sn nanoparticles on plastic using intense pulsed light annealing

Omar Kassem[1,2], Vincent Barnier[3], Mohamed Nasreldin[1], Jawad Reslan[1], Asdin Aoufi[3], Aravindnarain Ravichandran[1], Sergio Sao-joao[3], Khalid Hoummada[4], Ahmed Charai[4], Mathilde Rieu[2], Jean-Paul Viricelle[2], Thierry Djenizian[1,5], Mohamed Saadaoui[1*]

1. Mines Saint-Etienne, Center of Microelectronics in Provence, Department of Flexible Electronics, F-13541, Gardanne, France

2. Mines Saint-Etienne, Univ Lyon, CNRS, UMR 5307 LGF, Centre SPIN, F - 42023 Saint-Etienne France

3. Mines Saint-Etienne, Univ Lyon, CNRS, UMR 5307 LGF, Centre SMS, F - 42023 Saint-Etienne France

4. IM2NP, Faculté des Sciences de Saint-Jérôme case 142, Aix-Marseille University/CNRS, 13397, Marseille, France

5. Al-Farabi Kazakh National University, Center of Physical-Chemical Methods of Research and Analysis, Tole bi str., 96A. Almaty, Kazakhstan.

*Corresponding author: Dr. Mohamed Saadaoui   *E-mail*: saadaoui@emse.fr
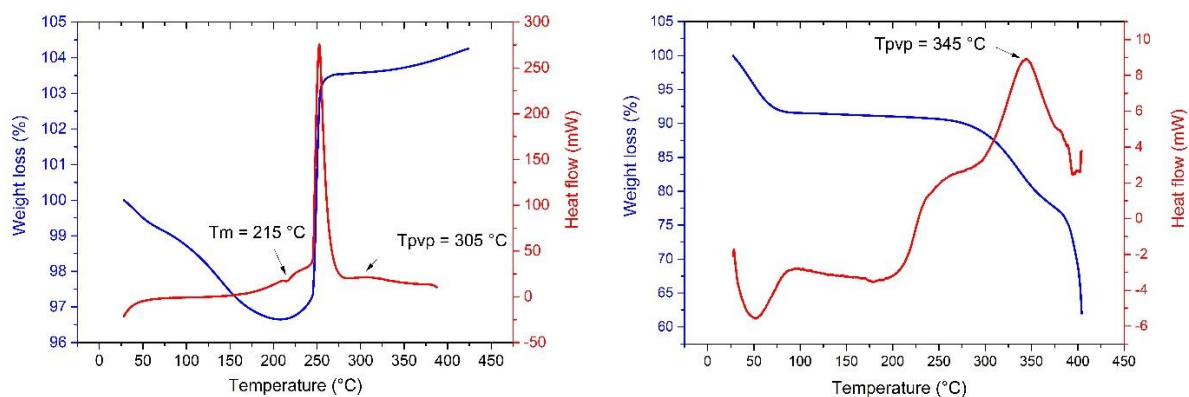
Figure S1 Simultaneous TGA/DSC curve of SnNPs (left) and pure PVP (right). The melting temperature of SnNPs is detected at 215 °C, 17°C below the melting depression of bulk Sn (Tm= 232 °C). The oxidation of SnNPs occurs before the start of the decomposition of the PVP (Tpvp=305°C).
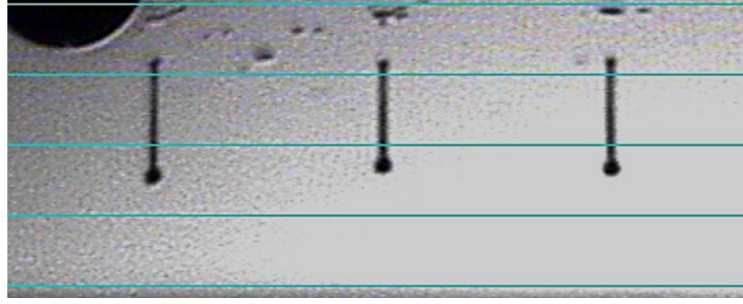
Figure S2 (a) Photograph of the 10% wt. SnNPs ink (b) Uniform flawless ejection of Sn ink using a jetting voltage of 17 V.

The surface energy is an essential parameter controlling the wettability of the ink on the substrate. The surface energy (γ_S) measurement of the Upilex foil was performed using Owens–Wendt–Rabel–Kaelble (OWRK) method[1], which is based on contact angle measurements of at least three reference liquids deposited on the substrate. γ_S is additively made up of dispersive γ_S^d and polar γ_S^p parts:

$$\gamma_S = \gamma_S^d + \gamma_S^p \tag{1}$$

γ_S could be extracted from the equation:

$$\gamma_L(1 + \cos\theta) = 2\sqrt{\gamma_L^d \gamma_S^d} + 2\sqrt{\gamma_L^p \gamma_S^p} \tag{2}$$

Where θ is the contact angle between the surface of the substrate and the liquid, γ_L is the surface tension of the liquid, γ_L^d is the dispersive surface tension and γ_L^p is the polar surface tension of the liquid. Using water, diiodomethane, ethylene glycol and a mixture of 40% ethylene glycol and 60% (Volume) of water as reference liquids, we found that the values of γ_S^d and γ_S^p are 41 mN/m and 6 mN/m, respectively. Therefore, γ_S of Upilex is found to be 47 mN/m. This value is higher enough than the surface tension of Sn ink, and thus will ensure good ink spreading on the substrate without the need for any surface treatment (Figure S2).
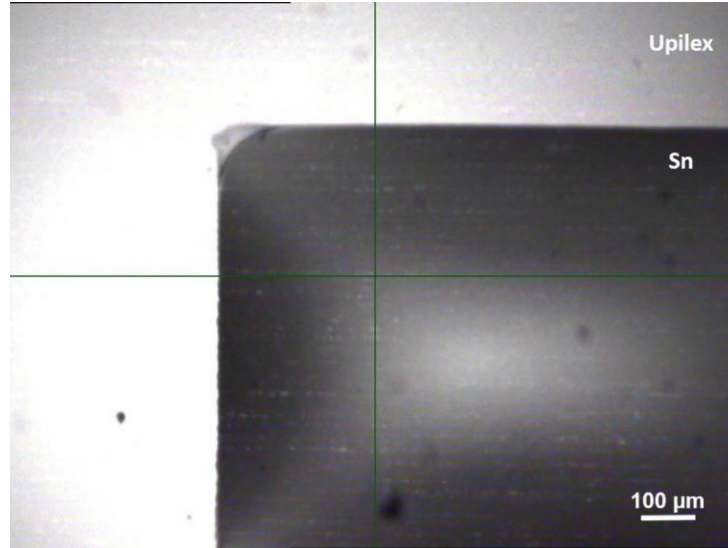
Figure S3 Optical micrograph of continuous and uniform Sn film, inkjet printed on Upilex (drop spacing 25 µm) observed by Dimatix printer camera.

The surface temperature during IPL was computed by solving the transient 1D nonlinear heat equation taking into account convection and radiation heat losses thanks to the finite volume method[2]. This conservative computational discretization method handles naturally the radiative boundary conditions which leads to solve a nonlinear system by the fixed point method, once a time implicit discretization was used. In order to ensure the conservation of the discrete heat flux across the boundary of two consecutive control volumes, a harmonic mean formula was used. At each step of the nonlinear solver, a tridiagonal system was solved by the standard TDMA (TriDiagonal Matrix Algorithm) technique.

A multilayer modelling was written which takes into account the temperature dependence of physical properties of both tin and Upilex. The emissivity was assumed constant.

On the first layer, the following heat equation can be written,

$$\rho_1 C p_1 \frac{\partial T_1}{\partial t}(x,t) = \frac{\partial}{\partial x}\left(K_1 \frac{\partial T_1}{\partial x}\right) \tag{3}$$

While on the second layer the heat equation can be written

$$\rho_2 C p_2\big(T_2(x,t)\big)\frac{\partial T_2}{\partial t}(x,t) = \frac{\partial}{\partial x}\left(K_2\big(T_2(x,t)\big)\frac{\partial T_2}{\partial x}\right) \tag{4}$$

The continuity of both temperature and heat flux at the interface between Upilex and tin located at x = e₁ was assumed in order to have a well posed modelling, this leads to the equations for t > 0,

$$T_1(e_1^-,t) = T_1(e_1^+,t) \; -K_1\frac{\partial T_1}{\partial x}(e_1^-,t) = -K_2\left(T_2(e_1^+,t)\right)\frac{\partial T_2}{\partial x}(e_1^+,t) \tag{5}$$

Finally two nonlinear boundary conditions were written at both ends of the geometry which take into account radiative and convective heat losses but also the absorbed power density provided by the xenon lamps.

$$K_1\frac{\partial T_1}{\partial x}(0,t) = Q(t) - h(T_1(0,t) - T_\infty) - \epsilon\sigma\big(T_1(0,t)^4 - T_\infty^4\big)$$
$$\tag{6}$$
$$- K_2\big(T_2(L,t)\big)\frac{\partial T_2}{\partial x}(L,t) = h(T_2(L,t) - T_\infty) + \epsilon\sigma\big(T_2(L,t)^4 - T_\infty^4\big)$$

Where Q=Q_abs is the transient heat flux absorbed by SnNPs ink that can be approximated by equation 7:

$$Q(x,t) = \frac{\int \alpha(\lambda)I(\lambda)d\lambda}{\int I(\lambda)d\lambda}\frac{P(t)}{\int P(t)dt}.E(x) \tag{7}$$

A set of two fiber-optic photodiodes (OSI optoelectronics OSI-515) was integrated for an in-situ recording of the emitted light intensity profile. Then, the emitted light power density 'P' was calculated by calibrating the emitted light intensity profile using energy density calculated by the bolometer.
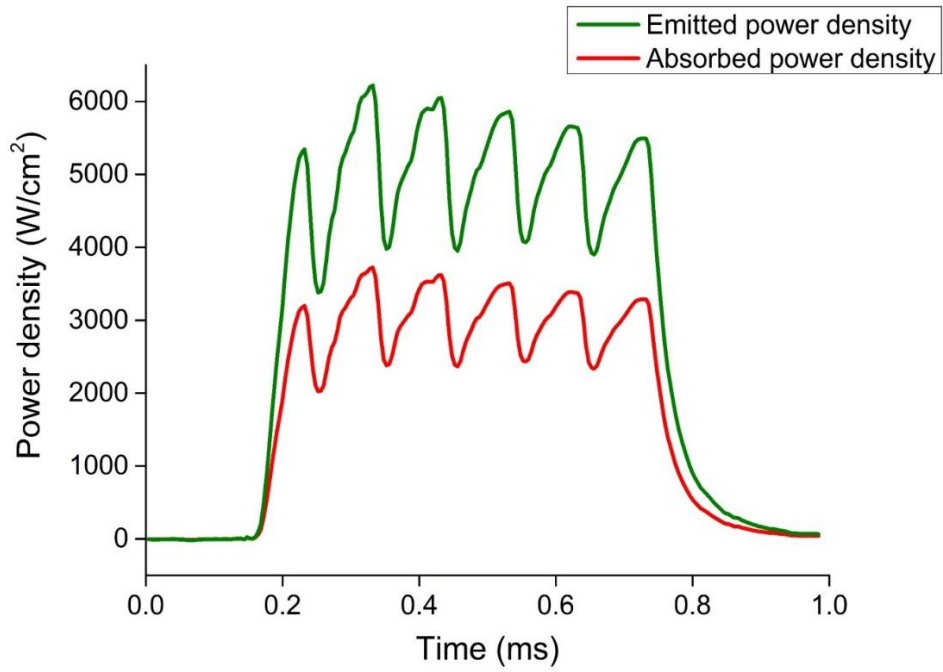
Figure S4. Power densities emitted by xenon lamps and absorbed by the Sn film for a set of 6 applied pulses (V = 360 V, Ton = 80 µs, Toff = 20 µs)

a)
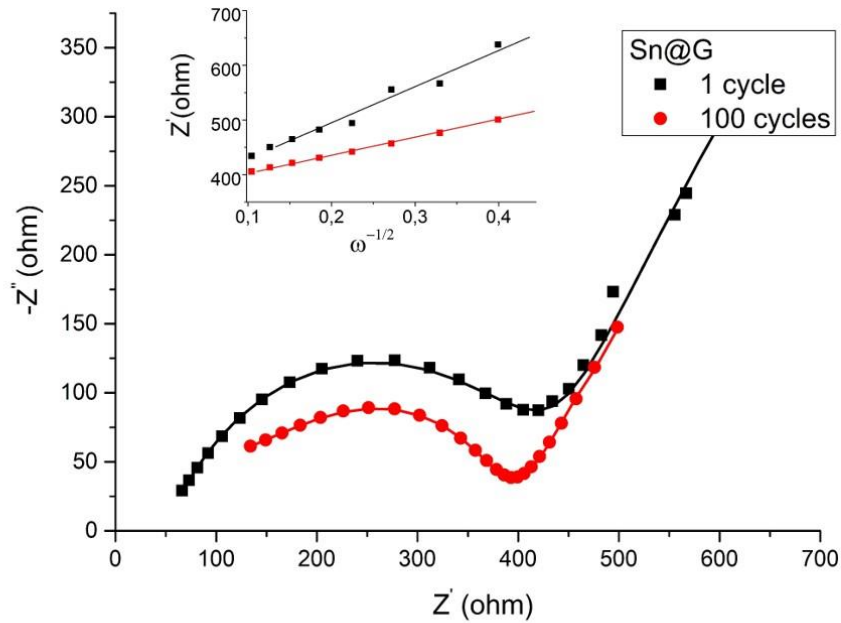
b)
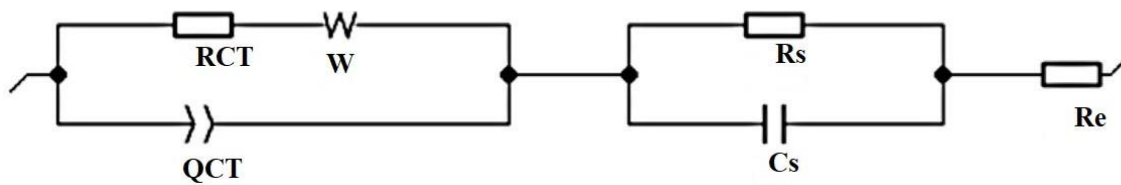
Figure S5. Electrochemical impedance spectroscopy of Sn@G electrode over the frequency range from 100 KHz to 0.9 Hz (a) Nyquist plot before after cycling at 1A/g (b) Randles equivalent circuit where Re is the resistance of the electrolyte, (R_S, C_S) is the resistance and the capacitance of SEI film, (R_{CT}, Q_{CT}) are the charge transfer resistance and constant phase element of the double layer, W is the Warburg impedance that simulate the diffusion of lithium ions into the bulk electrode.
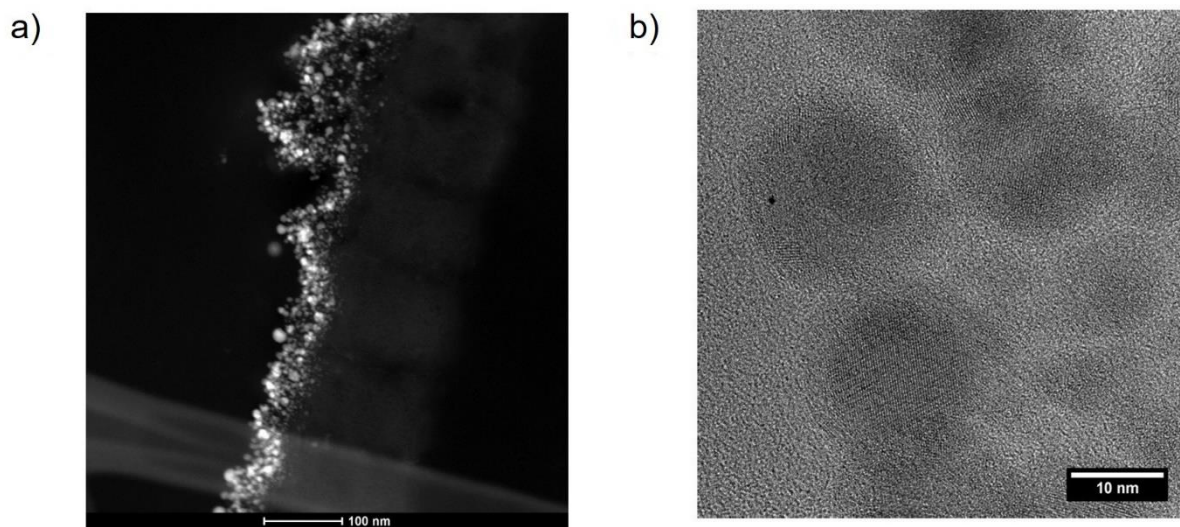
Figure S6. (a) STEM image of Sn@G electrode. (b) HRTEM images of some Sn@G particles after lithiation over 100 cycles at 1C. The Sn nanoparticles still keeps their initial diameter after lithiation without aggregation and pulverization
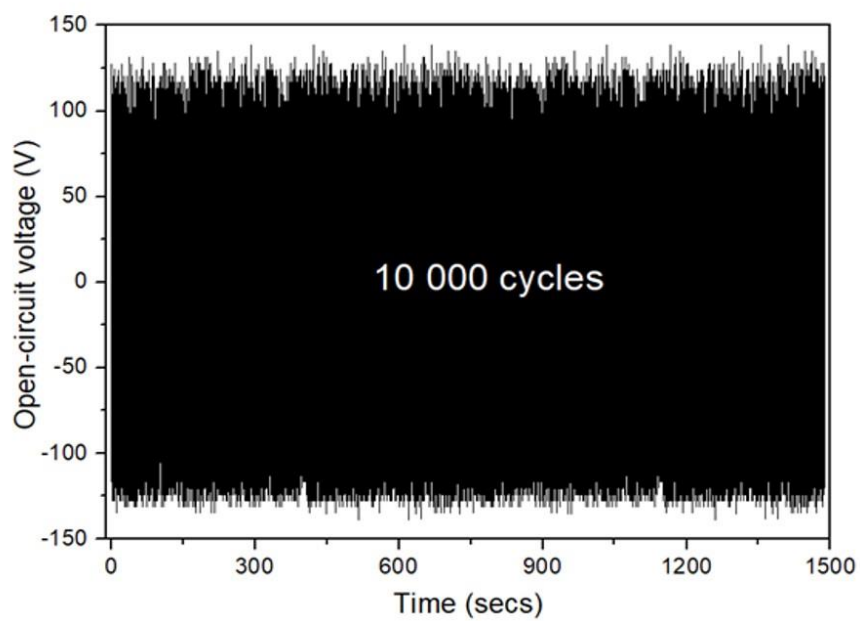
Figure S7 TENG stability test of the Sn@Gr during the 10,000 cycles.

Table S1. Thermal properties of Upilex[3] and Sn[4–7]

	Upilex®	Sn
ρ [Kg/m^3]	1470	7374.7 - 676.5x10^{-3} T
κ [W/m.K]	0.29	70 (T<Tmelt) and 17.37+0.023 T (T > Tmelt)
C_p [J/kg.K]	1130	351.4 – 322.5 x10^{-3}T + 229.1 x10^{-6}T^2
thickness (µm)	50	0.08
emissivity	0.95	0.25

Table S2. Summary of carbon sources and their ability to form Sn@G composite under IPL annealing

Substrate	Carbon source	Graphitization
Upilex® S	Upilex® S	Yes
Polyethylene terephtalate (PET)	Polyethylene terephtalate (PET)	No
Polyethylene naphtalate (PEN)	Polyethylene naphtalate (PEN)	No
Glass	Printed Polyimide ink (PI 6643-001)	Yes
Glass	Fructose	Yes

Table S3. Summary of the fitted parameters of the Sn@G electrodes

Sn@G	R_e (Ω)	R_{CT} (Ω)	σ (Ω rad$^{1/2}$s$^{-1/2}$)
1 cycle	44	480	670
100 cycles	42	352	360

Table S4. Literature review of performances of Sn/graphene hybrid material as anode for Lithium-ion batteries

Sn composite	Sn (wt %)	Intial discharge capacity	ICE	specific capacity mA/cm² (n cycle, current density)	Rate capacity (rate)	Voltage window (V, vs Li+/Li)	ref
Multilayer nanoassembly of Sn-nanopillar	70	945 at 50 mA	77.6	679 (30, 0.05A)	408 (5A)	0.002-3	8
Graphene Networks Anchored with Sn@Graphene	46.8	1805 at 200 mA	69	1089 (100, 0.2A) 657 (1000,2A)	270 (10A)	0.005-3	9
Graphene-Confined Sn Nanosheets	60.1	1380 at 50 mA	66.5	590 (60, 50 mA)	265 (1.6A)	0.005-2.0	10
Periodic structures of Sn self-inserted between graphene	60.6	1839 at 100 mA	77.7	838 (100, 0.1A) 684 (100, 0.5A) 693 (100, 1A)	398 (5A)	0.01-3	11
Tin Nanoparticles Impregnated in Nitrogen Sn@N-RGO	70	1211 at 100 mA	35	481 (100, 0.1A)	307 (2A)	0.005-3	12
Robust and stable intercalated graphene	42.5	2235 at 200 mA	79	846 (100, 0.2A)	488 (2A)	0.05-2	13
Decorating in situ ultrasmall tin particles on crumpled N-doped graphene	50	2028 at 100 mA	52	568 (1000, 1A)	340 (5A)	0.01- 2.5	14
Sn@graphene grown on vertically aligned graphene	60.7	1910 at 80 mA	54.2	1005 (120, 0.15A)	151 (166A)	0.001–3.0	15
Tin nanoparticles encapsulated in graphene backboned carbonaceous foams	56.5	-	-	777 (100, 0.1A) 506 (500, 0.4A)	270 (3.2A)	0.01-3.0	16
Dual-confinement via Sn@SnO2 core-shell nanoparticles embedded in 3D graphitized	58.6	1696 at 200 mA	52.4	725 (500, 1 A)	511 (5A/g)	0.01-3	17

Sn/graphene nanocomposite with 3D architecture	35	1250 at 80 mA	64.8	508 (100, 0.055A)	-	0.01-3	[18]
Organic molecule confinement reaction for preparation of the Sn nanoparticles@ graphene	19.58	901 at 100 mA 617 at 200 mA	67.8 64.5	539 (200, 0.1A) 407 (200, 0.2A)	240 (5A)	3	[19]
Stabilizing Sn anodes nanostructure: Structure optimization and interfacial engineering to boost lithium storage	85.5	1548 at 500 mA	74.8	1236.5 (150, 0.5A) 1083.9 (500 at 1A)	502.8 (20A)	0.01–3.0	[20]
SnNP@G [This work]	20	2205 at 100 mA	50	1017 (100, 1)	760 (0.5A)	0.002-3	

Table S5. Some literature review of performances of TENG devices made out of graphene and graphene composite materials

Electrode / Triboelectric material	Current (µA)	Voltage (V)	Max power density (mW/m²)	Ref
Gr / PET / Gr	-	9	25	[21]
Gr / PDMS / Gr	0.9	22	-	[22]
Gr / PTFE / Gr	7.2	128	-	[23]
Gr / Parylene / Gr	0.02	3	-	[24]
Gr / Nylon/ Gr	-	250	290	[25]
ITO-Gr / Gr-PDMS	12	650	20.8	[26]
Gr-PVDF / Gr-Nylon	-	-	4.4	[27]
Sn@G / PI / Sn@G [This work]	5.8	150	125	

References

(1) Kassem, O.; Saadaoui, M.; Rieu, M.; Sao-Joao, S.; Viricelle, J. P. Synthesis and Inkjet Printing of Sol–Gel Derived Tin Oxide Ink for Flexible Gas Sensing Application. J. Mater. Sci. 2018, 53 (18), 12750–12761.

(2) Patankar, S. Numerical Heat Transfer and Fluid Flow; McGraw-Hill, New York, 1980.

(3) https://www.ube.com/upilex/en/upilex.html. https://www.ube.com/upilex/en/upilex.html.

(4) Alchagirov, B. B.; Chochaeva, A. M. Temperature Dependence of the Density of Liquid Tin. High Temp. 2000, 38 (1), 44–48. https://doi.org/10.1007/BF02755565.

(5) Dutchak, Ya. I.; Osipenko, V. P.; Panasyuk, P. V. Thermal Conductivity of Sn-Bi Alloys in the Solid and Liquid States. Sov. Phys. J. 1968, 11 (10), 145–147. https://doi.org/10.1007/BF00822489.

(6) Chapman, T. W. The Heat Capacity of Liquid Metals. Mater. Sci. Eng. 1966, 1, 65–69.

(7) Assael, M. J.; Chatzimichailidis, A.; Antoniadis, K. D.; Wakeham, W. A.; Huber, M. L.; Fukuyama, H. Reference Correlations for the Thermal Conductivity of Liquid Copper, Gallium, Indium, Iron, Lead, Nickel and Tin. High Temp High Press 2017, 391-416.

(8) Ji, L.; Tan, Z.; Kuykendall, T.; An, E. J.; Fu, Y.; Battaglia, V.; Zhang, Y. Multilayer Nanoassembly of Sn-Nanopillar Arrays Sandwiched between Graphene Layers for High-Capacity Lithium Storage. Energy Environ. Sci. 2011, 4 (9), 3611. https://doi.org/10.1039/c1ee01592c.

(9) Qin, J.; He, C.; Zhao, N.; Wang, Z.; Shi, C.; Liu, E.-Z.; Li, J. Graphene Networks Anchored with Sn@Graphene as Lithium Ion Battery Anode. ACS Nano 2014, 8 (2), 1728–1738. https://doi.org/10.1021/nn406105n.

(10) Bin, L.; Bin, W.; Xianglong, L.; Yuying, J.; Minghui, L.; Linjie, Z. Graphene-Confined Sn Nanosheets with Enhanced Lithium Storage Capability. Adv. Mater. 2012, 24 (41), 5525–5525.

(11) Zhou, X.; Zou, Y.; Yang, J. Periodic Structures of Sn Self-Inserted between Graphene Interlayers as Anodes for Li-Ion Battery. J. Power Sources 2014, 253, 287–293. https://doi.org/10.1016/j.jpowsour.2013.12.034.

(12) Zhou, X.; Bao, J.; Dai, Z.; Guo, Y.-G. Tin Nanoparticles Impregnated in Nitrogen-Doped Graphene for Lithium-Ion Battery Anodes. J. Phys. Chem. C 2013, 117 (48), 25367–25373. https://doi.org/10.1021/jp409668m.

(13) Wang, C.; Ju, J.; Yang, Y.; Tang, Y.; Bi, H.; Liao, F.; Lin, J.; Shi, Z.; Huang, F.; Han, R. P. S. Robust and Stable Intercalated Graphene Encapsulation of Tin Nanorods for Enhanced Cycle and Capacity Performance for Lithium Storage. RSC Adv. 2013, 3 (44), 21588. https://doi.org/10.1039/c3ra44109a.

(14) Liu, L.; Huang, X.; Guo, X.; Mao, S.; Chen, J. Decorating in Situ Ultrasmall Tin Particles on Crumpled N-Doped Graphene for Lithium-Ion Batteries with a Long Life Cycle. J. Power Sources 2016, 328, 482–491. https://doi.org/10.1016/j.jpowsour.2016.08.033.

(15) Li, N.; Song, H.; Cui, H.; Wang, C. Sn@graphene Grown on Vertically Aligned Graphene for High-Capacity, High-Rate, and Long-Life Lithium Storage. Nano Energy 2014, 3, 102–112. https://doi.org/10.1016/j.nanoen.2013.10.014.

(16) Luo, B.; Qiu, T.; Ye, D.; Wang, L.; Zhi, L. Tin Nanoparticles Encapsulated in Graphene Backboned Carbonaceous Foams as High-Performance Anodes for Lithium-Ion and Sodium-Ion Storage. Nano Energy 2016, 22, 232–240. https://doi.org/10.1016/j.nanoen.2016.02.024.

(17) Fan, B.; Liu, J.; Xu, Y.; Tang, Q.; Zhang, Y.; Chen, X.; Hu, A. A Facile Strategy towards High Capacity and Stable Sn Anodes for Li-Ion Battery: Dual-Confinement via

Sn@SnO2 Core-Shell Nanoparticles Embedded in 3D Graphitized Porous Carbon Network. J. Alloys Compd. 2021, 857, 157920. https://doi.org/10.1016/j.jallcom.2020.157920.

(18)   Wang, G.; Wang, B.; Wang, X.; Park, J.; Dou, S.; Ahn, H.; Kim, K. Sn/Graphene Nanocomposite with 3D Architecture for Enhanced Reversible Lithium Storage in Lithium Ion Batteries. J. Mater. Chem. 2009, 19 (44), 8378. https://doi.org/10.1039/b914650d.

(19)   Ding, S.; Cheng, W.; Zhang, L.; Du, G.; Hao, X.; Nie, G.; Xu, B.; Zhang, M.; Su, Q.; Serra, C. A. Organic Molecule Confinement Reaction for Preparation of the Sn Nanoparticles@graphene Anode Materials in Lithium-Ion Battery. J. Colloid Interface Sci. 2021, 589, 308–317. https://doi.org/10.1016/j.jcis.2020.12.086.

(20)   Kong, Z.; Zhang, K.; Huang, M.; Tu, H.; Yao, X.; Shao, Y.; Wu, Y.; Hao, X. Stabilizing Sn Anodes Nanostructure: Structure Optimization and Interfacial Engineering to Boost Lithium Storage. Electrochimica Acta 2022, 405, 139789. https://doi.org/10.1016/j.electacta.2021.139789.

(21)   Seongsu, K.; Manoj Kumar, G.; Keun Young, L.; Dong-Wook, K.; Sang-Woo, K. Transparent Flexible Graphene Triboelectric Nanogenerators. Adv. Mater. 2014, 26 (13), 3918–3925.

(22)   Bananakere Nanjegowda, C.; Bing, D.; Ankanahalli Shankaregowda, S.; Hailin, P.; Zhongfan, L. Roll-to-Roll Green Transfer of CVD Graphene onto Plastic for a Transparent and Flexible Triboelectric Nanogenerator. Adv. Mater. 2015, 27 (35), 5210–5216.

(23)   Zhao, X.; Zhang, D.; Xu, S.; Qian, W.; Han, W.; Wang, Z. L.; Yang, Y. Stretching-Enhanced Triboelectric Nanogenerator for Efficient Wind Energy Scavenging and Ultrasensitive Strain Sensing. Nano Energy 2020, 75, 104920. https://doi.org/10.1016/j.nanoen.2020.104920.

(24)   Z. Liu, Z. Zhao, X. Zeng, X. Fu, Y. Hu.; Ultrathin, flexible and transparent graphene-based triboelectric nanogenerators for attachable curvature monitoring,. J. Phys. D Appl. Phys. 52 (2019)

(25)   G. Pace, A. Ansaldo, M. Serri, S. Lauciello, F. Bonaccorso, Electrode selection rules for enhancing the performance of triboelectric nanogenerators and the role of few-layers graphene, Nano Energy 76 (2020) https://doi.org/10.1016/j.nanoen.2020.104989, 104989

(26)   S. A. Shankaregowda, C. B. Nanjegowda, X.-L. Cheng, M.-Y. Shi, Z.-F. Liu, H.-X. Zhang. A Flexible and Transparent Graphene-Based Triboelectric Nanogenerator. IEEE Trans. Nanotechnol. 2016, 15, 435.

(27)   Pace G, Serri M, del Rio Castillo AE, et al. Nitrogen-doped graphene based triboelectric nanogenerators. Nano Energy. 2021;87:106173. https://doi.org/10.1016/j.nanoen.2021.106173